Modeling electroporation of the non-treated and vacuum impregnated heterogeneous tissue of spinach leaves

Dymek, Katarzyna; Rems, Lea; Zorec, Barbara; Dejmek, Petr; Gomez, Federico; Miklavcic, Damijan

Published in:
Innovative Food Science & Emerging Technologies

DOI:
10.1016/j.ifset.2014.08.006

2015

Innovative Food Science and Emerging Technologies 29 (2015) 55–64

Contents lists available at ScienceDirect

Innovative Food Science and Emerging Technologies

journal homepage: www.elsevier.com/locate/ifset

Modeling electroporation of the non-treated and vacuum impregnated heterogeneous tissue of spinach leaves

Katarzyna Dymek [a,*], Lea Rems [b], Barbara Zorec [b], Petr Dejmek [a], Federico Gómez Galindo [a], Damijan Miklavčič [b]

[a] Food Technology, Engineering and Nutrition, Lund University, PO Box 124, SE-221 00 Lund, Sweden
[b] Faculty of Electrical Engineering, University of Ljubljana, Trzaska 25, SI-1000 Ljubljana, Slovenia

ARTICLE INFO

Article history:
Received 24 May 2014
Accepted 25 August 2014
Available online 30 August 2014

Keywords:
Spinach leaf
Electroporation
Numerical modeling
Vacuum impregnation

ABSTRACT

Uniform electroporation of the heterogeneous structure of spinach leaf cross section is a technological challenge that is addressed in this investigation. Three dimensional models were created with cells arranged in specific tissue types, considering a leaf with its air fraction and a leaf where the air fraction was replaced by a solution of known properties using vacuum impregnation. The models were validated before electroporation, in the frequency domain, where alternating voltage and current signal at frequencies from 20 Hz to 1 MHz were used to measure conductivity of the tissue. They were also validated through measurements of current during electroporation when a single 250 μs rectangular pulse with amplitudes ranging from 50 to 500 V was applied. Model validations show that both the frequency dependent conductivity and electroporation are well predicted. The importance of the wax layer and stomata in the model is thoroughly discussed.

Industrial relevance: Our aim was to investigate electroporation of the spinach leaf by developing a model which would enable us to meet the technological challenge of achieving uniform electroporation in a highly heterogeneous structure in the context of a process aimed at improving freezing stability of plant foods. Pulsed electric field treatment may be used to introduce the cryoprotectant molecules into the cells, and hence improve the structure and properties of frozen food plants.

1. Introduction

Electroporation of a cell membrane is defined as an increase in its permeability due to exposure of the cell to a sufficiently strong, external electric field (Kotnik, Kramar, Pucihar, Miklavcic, & Tarek, 2012; Neumann & Rosenheck, 1972; Neumann, Schaefer-Ridder, Wang, & Hofschneider, 1982; Zimmermann, Pilwat, & Riemann, 1974; Zimmermann & Vienken, 1982). Depending on the amplitude and duration of the applied electric field, electroporation may occur in two forms: irreversible (Phillips, Maor, & Rubinsky, 2011; Rowan, MacGregor, Anderson, Fouracre, & Farish, 2000) or reversible (Glaser, Leikin, Chernomordik, Pastushenko, & Sokirko, 1988; Miklavčič, Serša, Brecelj, Gehl, Soden, Bianchi, et al., 2012). For either purpose, theoretical studies coupled with experimental investigation contribute to the understanding of events taking place in cells and tissues during electroporation.

Theoretical studies of single cell electroporation have been conducted from different perspectives. Aspects such as the dynamics of pore formation and the transmembrane voltage distribution (DeBruin & Krassowska, 1999), the electroporation caused by bipolar pulses and dynamic pore radii (Talele, Gaynor, Cree, & van Ekeran, 2010), the conductance of electroporated cell membrane (Suzuki, Ramos, Ribeiro, Cazarolli, Silva, Leite, et al., 2011), the number of pores and pore radii in the cell membrane (Talele & Gaynor, 2010), the process of pore disappearance in the cell membrane (Saulis, 1997) and the electroporation of intracellular membranes (Gowrishankar, Esser, Vasilkoski, Smith, & Weaver, 2006; Retelj, Pucihar, & Miklavcic, 2013) have been widely studied in the literature using single cell models. Electroporation was also studied by using a model of dense cell suspension (Mezeme, Pucihar, Pavlin, Brosseau, & Miklavčič, 2012).

Electroporation of tissues has attracted great attention. Electroporation is an important technology used for medical purposes such as cancer treatment (electrochemotherapy) (Yarmush, Golberg, Serša, Kotnik, & Miklavčič, 2014), where the modeling of the electroporation process in the tissue becomes essential for treatment planning (Pavliha, Kos, Zupanič, Marčan, Serša & Miklavčič, 2012; Pavšelj & Miklavčič, 2008). In these models describing tissue electroporation, the representation of the heterogeneity and anisotropy of the tissues becomes a challenge. There are number of models describing electroporation in different types of tissues such as tumors, muscle, liver and skin, where the heterogeneous tissue layers are considered and the thermal effects of electroporation and transdermal drug delivery are studied (Pavšelj & Miklavčič, 2011; Zorec, Becker, Reberšek, Miklavčič, & Pavšelj, 2013). Electroporation of skin was also studied in terms of the effect of bipolar pulses (Arena, Sano, Rylander, & Davalos, 2011). Three dimensional models were used to evaluate the local electric field created

* Corresponding author. Tel.: +46 462229806; fax: +46 4622 24622.
E-mail address: katarzyna.dymek@food.lth.se (K. Dymek).

http://dx.doi.org/10.1016/j.ifset.2014.08.006
1466-8564/

in the anisotropic skeletal muscle during the application of electric pulses (Corovic, Zupanic, Kranjc, Al Sakere, Leroy-Willig, Mir, et al., 2010) and two dimensional models of nerves, blood vessels and ducts have been used to theoretically analyze irreversible electroporation (Daniels & Rubinsky, 2009).

The models describing electroporation are however mostly focused on a simplified geometry which shows the tissues as stacks of layers with specific bulk properties. In this paper we use a three dimensional model, containing a well-defined structure built from individual cells arranged in specific tissue types. Cells belonging to a certain tissue possess shape, dimensions and location mimicking the tissues in the real spinach leaf. The entire cross section of the leaf was considered including elements such as the cuticular wax and stomata.

Our aim was to investigate electroporation of the spinach leaf cross section by developing a model which would enable us to meet the technological challenge of achieving uniform electroporation in a highly heterogeneous structure in the context of a process aimed at improving freezing stability of plant foods (Phoon, Gómez Galindo, Vicente, & Dejmek, 2008; Shayanfar, Chauhan, Toepfl, & Heinz, 2013). The influence of specific elements such as cell size, cell arrangement, cuticular wax layer and stomata on the creation of pores (i.e. electroporation of the cell membranes under different applied pulse parameters), was investigated. The effects of the connections between cells and the air fraction in the tissue are also discussed. The model was first analyzed in the frequency domain, where alternating voltage and current signal at frequencies from 20 Hz to 1 MHz were used to measure conductivity in the tissue and validate the model.

2. Theoretical considerations

2.1. Spinach leaf structure

Spinach leaf has a typical thickness of 0.4 ± 0.1 mm. The cross section of the leaf consists of different tissues arranged in four layers. The spinach cross section is shown in Fig. 1A, where leaves were incubated with fluorescein diacetate as described by Dymek, Dejmek, and Gómez Galindo (2014) and examined under a microscope (Eclipse Ti-U, Nikon, Japan). At the top of the leaf cross section there is an upper epidermal tissue, which consists of a single layer of star-shaped cells. Epidermal cells are covered by a cuticular wax layer. Underneath the upper epidermis the palisade mesophyll is built from elongated cells which are formed by two cell layers. Below the palisade mesophyll, the spongy mesophyll is located. It has a multi-cell layer structure characterized by round cells distributed in a loose and apparently random structure. The majority of the intercellular air fraction is located in the spongy mesophyll (Warmbrodt & Woude, 1990). The air fraction accounts for approximately 30% of the leaf volume (Winter, Robinson, & Heldt, 1994). At the bottom, the lower epidermis is located.

2.2. Simplifications used to model the leaf

The model represents the internal tissues of a spinach leaf, restricting the elements included in the model to the essential ones. The leaf tissue possesses an extremely complex structure; therefore, the following simplifications were introduced into the model.

Veins were not included in the model. Since obtaining a time-dependent, finite-element solution for a 3D model with a complex structure consisting of multiple cells is relatively demanding with respect to computational time and random-access memory requirement, only a small part of the leaf with an area 107 μm × 107 μm was modeled. In the spinach leaf the minor veins are located within the distance from 49 to 231 μm (Warmbrodt & Woude, 1990) and were neglected in the model.

In the leaf the majority of the air fraction is located in the spongy mesophyll. Therefore, in the model, air fraction was neglected in the epidermal tissue and palisade mesophyll. In these tissues the cells were completely surrounded by extracellular liquid. However, in the spongy mesophyll the cells were surrounded by a thin layer of

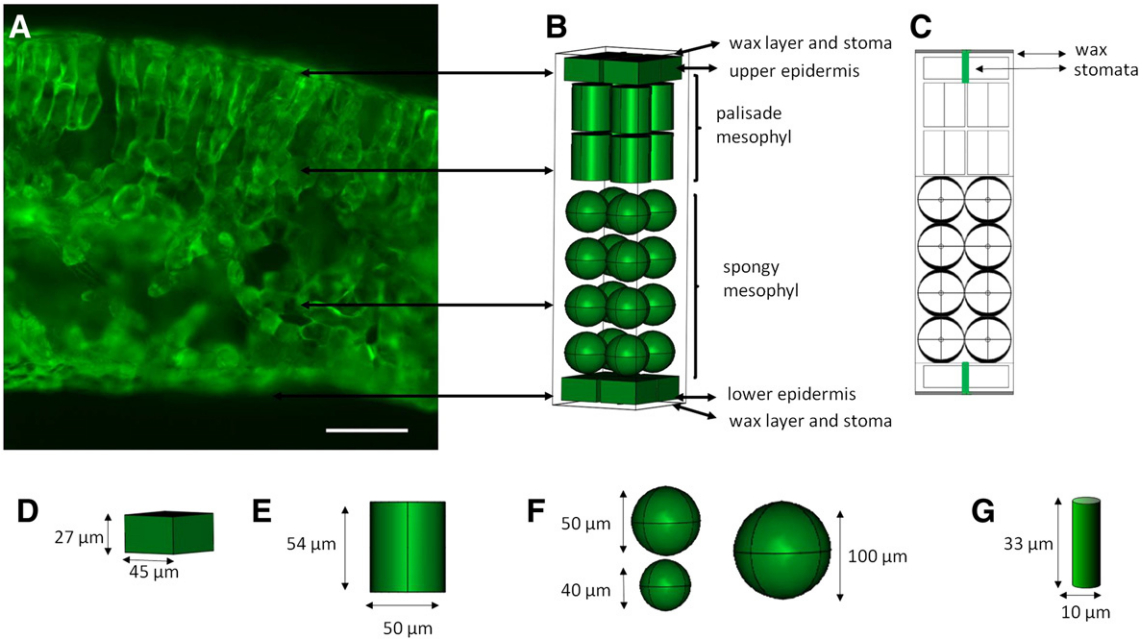

Fig. 1. The geometry of the model. A, B. The geometry of the model representing the whole spinach cross section is shown in relation with the microscopic picture. The scale bar represents 100 μm. C. Side view of the model with connections between cells marked with black. Stomata are marked in green and the cuticular wax layer in black. The dimensions of the different elements included in the model are shown in: D. epidermal cell, E. palisade mesophyll cell, F. spongy mesophyll cells, G. stoma.

extracellular liquid, which mimics the apoplastic pathway (space between the cell membrane and the cell wall) and connects all the cells in the spongy mesophyll. This thin layer was then directly surrounded by air, avoiding the need to specifically include the cell walls.

The shape of the epidermal cells was also simplified to avoid a too complex structure leading to excessive number of finite elements in the model and meshing problems. In the spinach leaf, epidermal cells are star-shaped, whereas in the model they are represented as blocks.

3. Numerical model

COMSOL Multiphysics 3.5a (COMSOL AB, Stockholm, Sweden), a commercial finite element software package, was used to perform calculations of the leaf conductivity at different frequencies when AC voltage was applied, and to simulate pore formation in the cell membranes when DC voltage (electroporative electric pulse) was applied.

3.1. Geometry of the model

The model of the spinach leaf cross section was created based on microscopic pictures from previously published papers (Warmbrodt & Woude, 1990; Winter, Robinson & Heldt, 1994) as well as our observations and measurements.

The model represents a part of the spinach leaf with an area of 107 μm × 107 μm and thickness of 420 μm. Fig. 1B shows how the cells were arranged in the four tissue layers: lower and upper epidermis and mesophyll differentiated into palisade and spongy cells. The proportions of the tissues were based on the micrographs (Warmbrodt & Woude, 1990; Winter, Robinson & Heldt, 1994). Epidermal cells were presented as blocks with dimensions of 45 μm × 45 μm × 27 μm (Fig. 1D). There was a single layer with four epidermal cells located at the bottom and top of the leaf. Palisade mesophyll cells were presented as 54 μm long cylinders having a diameter of 50 μm (Fig. 1E). They were arranged in two layers, each consisting of four cells. Spongy mesophyll is the most irregularly structured tissue due to its high air fraction. Therefore, to examine the influence of the cell distribution and size on the electrical properties of the spinach leaf, three models with different arrangements of spongy mesophyll cells were built, as shown in Fig. 2. Model A contained two large spongy mesophyll cells with a diameter of 100 μm; model B contained 4 rows of cells having a diameter of 50 μm, with 4 cells placed in each of the rows; and model C contained randomly located spongy mesophyll cells with two different diameters: 50 and 40 μm.

Additionally, model D was built, which had the same cell arrangement as model B. However, at the top and bottom of the leaf there were also 0.3 μm thick cuticular wax layers (Hardin, Jones, Weckler, Maness, Dillwith, & Madden, 2013; Riederer & Schreiber, 2001) (Fig. 1C). Both wax layers contained ellipsoidal holes filled with air (10 μm long and 4.5 μm wide), which were extended further into the epidermal tissue in the shape of elliptic cylinders, representing the stomata (Fig. 1C and G, marked with green).

3.2. Connections between cells

The proper function of the whole plant organism is enabled by connections between cells. Since the cells are surrounded by non-conductive air fraction, their connections influence significantly the current flow through the tissues. In the model, the air fraction was included only in the spongy mesophyll. To model the connections between cells (the apoplastic pathway), in each of the different models (A, B, C and D) the spongy mesophyll cells were surrounded by a thin layer of extracellular fluid (shown in black in Fig. 1C and also in white in side views of the models in Fig. 2). This layer was built by slightly increased and elongated elements overlapping each other at the poles; the minimum thickness of the layer was 0.5 μm, whereas at the poles of the spongy cells, its thickness was increased to 4 μm, to allow connecting the cells. The rest of the volume in spongy mesophyll was filled with air. The interface between the layer representing the apoplastic pathway and the air then mimicked the cell walls.

Another model was built representing a vacuum impregnated leaf, where the air fraction was removed and all cells were surrounded by an external solution of known properties, resulting in a continuously conductive pathway trough the leaf. In this case, the connections between cells were neglected. The cell walls could be omitted as well, because they influence neither the electroporation process nor the transport of small molecules (Kandušer, & Miklavčič, 2008).

3.3. Model parameters

To model the electrodes, an electric potential was assigned to the upper and lower boundaries of the leaf model. One side was grounded and the other was excited by a single, rectangular 250 μs pulse with amplitudes ranging from 50 to 500 V. The pulse was modeled as described by Retelj, Pucihar and Miklavcic (2013) using the COMSOL function flc1hs. The pulse rise and fall times were set to 1 μs. The vertical sides of the model were modeled as electrically insulated. Mathematical

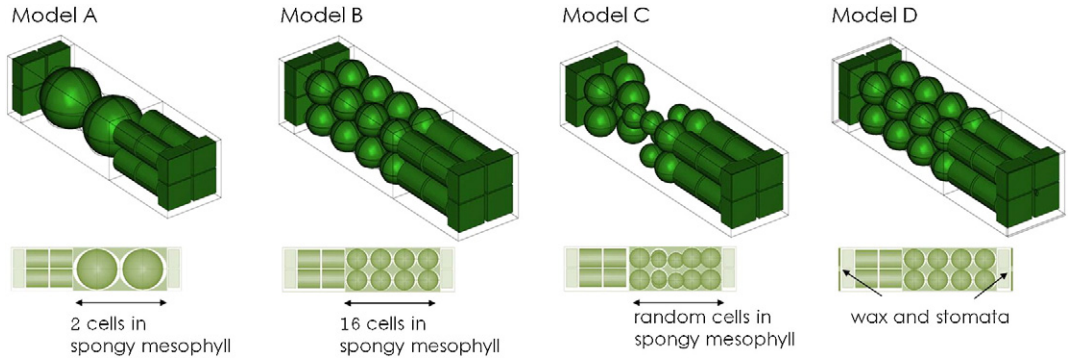

Fig. 2. The geometry of investigated models of untreated spinach leaf cross section with highlighted main differences between models. The three dimensional view as well as the schematic side view of the models is shown. Model A. The model represents the spinach leaf cross section with two large cells in the spongy mesophyll tissue. Model B. The model represents the spinach leaf cross section with 16 cells in the spongy mesophyll tissue arranged in the 4 rows with 4 cells per row. Model C. The model represents the spinach leaf cross section with randomly located cells in the spongy mesophyll tissue. Model D. The model represents the spinach leaf cross section with 16 cells in the spongy mesophyll tissue arranged in the 4 rows with 4 cells per row, the same as model B, but in model D also the cuticular wax layers and stomata are included.

equations describing electroporation of the cell membrane were taken from DeBruin and Krassowska (1999) and the method for calculating the induced transmembrane voltage was adopted from Pucihar, Miklavcic, and Kotnik (2009). Electric potential V was calculated by

$$-\nabla(\sigma_i \nabla V) - \nabla \frac{\partial(\varepsilon_i \nabla V)}{\partial t} = 0 \quad (1)$$

where σ_i and ε_i are the conductivity and dielectric permittivity, respectively. The cell membrane was modeled using *Distributed Impedance* boundary condition by

$$\boldsymbol{n} \cdot \boldsymbol{J} = \frac{\sigma_m}{d_m}\left(V - V_{ref}\right) + \frac{\varepsilon_m}{d_m}\left(\frac{\partial V}{\partial t} - \frac{\partial V_{ref}}{\partial t}\right) \quad (2)$$

where $\boldsymbol{J}$ is the current density through the cell membrane, $\boldsymbol{n}$ is the unit vector normal to the membrane surface, V and V_{ref} are the potentials on each side of the membrane, d_m is the membrane thickness, σ_m is the membrane conductivity and ε_m is the membrane dielectric permittivity. A difference between the electric potential on each side of the boundary gives the induced transmembrane voltage (ITV).

The differential equation describing the dynamics of pore formation is

$$\frac{dN}{dt} = \alpha e^{\left(\frac{ITV}{V_{ep}}\right)^2}\left(1 - \frac{N}{N_0} e^{-q\left(\frac{ITV}{V_{ep}}\right)^2}\right) \quad (3)$$

where N is the pore density, N_0 is the pore density in non-electroporated cell membrane and α, q and V_{ep} are electroporation parameters. Formation of pores considerably increases the conductivity of the cell membrane. This increase in conductivity due to electroporation can be calculated as (DeBruin & Krassowska, 1999)

$$\sigma_{ep} = \pi r_p^2 \sigma_p N \frac{e^V m - 1}{\frac{we^{w-nV}m - nV_m}{w - nV_m} e^{V_m} - \frac{we^{w-nV}m + nV_m}{w + nV_m}} \quad (4)$$

where r_p is the radius and σ_p is the internal conductivity of a pore. $V_m = ITV \cdot F/(R \cdot T)$ is the nondimensional transmembrane voltage, where F is the Faraday constant, R is the universal gas constant, and T is the temperature. Parameter n represents the length of pore entrance area, and w accounts for the energy cost for moving an ion from a region of high dielectric constant (water) to a small pore in the lipid bilayer with low dielectric constant. The total membrane conductivity, as used in Eq. (2), is then calculated in each time step as the sum of the passive membrane conductivity (given in Table 1) and σ_{ep}.

The conductivity and relative permittivity of the particular elements, such as cytoplasm and cell membranes, were set according to the published data and are listed in Table 1.

4. Measurements

4.1. Raw material

Spinach leaves were collected from the local supermarket. Leaves were stored at 1–2 °C in closed plastic bags and used for experiments until the expiration date established by the producer (9 days from the packaging date). Leaves of similar size (6 ± 0.5 cm long and 2.5 ± 0.3 cm wide) were selected for the experiments.

4.2. Measurements of leaf electric conductivity

Samples (1 cm × 1 cm) were cut from the leaf. Each sample was cut in the same spot at the center of the leaf, from the central vein towards the edge. Samples were immersed in a 0.25 S/m PBS buffer (Phosphate Buffered Saline) and placed between two flat stainless steel electrodes, which were smaller than the sample, hence a leaf area of 64 mm^2 was enclosed between the electrodes. Conductivity of the PBS was measured with a conductivity meter (Orion 150, Orion Research Inc., Jacksonville, FL, USA). Electrodes were squeezed with a plastic clamp and connected to an impedance analyzer (4192A LF, Hewlett Packard, California, USA). A sinusoidal signal of 1 V amplitude was applied to the leaf samples and the resistance (in Ohms) was recorded at frequencies from 20 Hz to 1 MHz. The measurement was done for untreated samples (with air fraction) and for samples after vacuum impregnation (without air fraction).

4.2.1. Evaluation of the effect of the air fraction on leaf electric conductivity

To determine the influence of the air fraction on the electrical properties of the spinach leaf and to analyze the importance of its presence in the model, the air fraction of the leaf was removed and replaced by an external solution using vacuum impregnation.

Three leaves were immersed in 100 ml PBS buffer with conductivity of 0.25 S/m. Immersed leaves were placed in a vessel connected to a vacuum pump and vacuum controller (S.I.A., Bologna, Italy) as described by Panarese, Dejmek, Rocculi and Gómez Galindo (2013). The pressure was decreased to 150 mbar in 3.5 min. It was kept constant at 150 mbar for 1 min and increased for 4.5 min until atmospheric pressure was recorded. Samples were kept under atmospheric pressure for 10 min. The entire cycle was repeated twice (Demir, 2012). The relative increase in the leaf mass after vacuum impregnation was 39 ± 5%.

4.3. Measurements of current changes during electroporation

Leaves were placed between two flat stainless steel electrodes. The gap between electrodes was 4 mm and it was filled with PBS buffer of conductivity 0.25 S/m. The area of the leaf samples enclosed between the electrodes was 64 mm^2. A single electric pulse of 250 μs with amplitude of 50, 100, 200, 300, 400 or 500 V was applied. The pulse was delivered by a CEPT® electroporator (ARC AROMA PURE, Lund, Sweden). The current was recorded by a scopemeter (Fluke 123, Industrial Scopemeter, Washington, USA) equipped with a current probe.

5. Results and discussion

5.1. Influence of the cell size, cell arrangement, cuticular wax layer and stomata on the frequency-dependent conductivity of the spinach leaf model

Results obtained using models A–C (Fig. 2) were compared with measurements of the frequency-dependent conductivity of the spinach leaves (Fig. 3). When comparing models A–C with experimental measurements, it can be clearly seen that the models resulted in higher conductivity values for frequencies lower than 10 kHz and failed to predict the increase in conductivity measured from 100 kHz to 1 MHz. Furthermore, results obtained from models A, B and C show that the influence of the spongy mesophyll cell size and cell arrangement on the calculated conductivity is not significant. Two large cells located in the spongy mesophyll (Fig. 2, model A) showed a very similar conductivity (differed by 0.15 mS/m) as 16 cells located in the spongy mesophyll (Fig. 2, model B) at 10 Hz. Randomly located cells (Fig. 2, model C) resulted in slightly lower conductivities.

Model D (Fig. 2) contains additional elements to model B: cuticular wax layer and stomata, which has a significant influence on the overall electrical properties of the spinach leaf. Model D resulted in conductivity values increasing from 0.56 mS/m at 10 Hz to 4 mS/m at 1 MHz and was thus the only one able to predict (at least qualitatively) the measured increase in conductivity with increasing frequency. This clearly demonstrates that the electrical properties of the cuticular wax layer predominantly determine the properties of the leaf in the observed frequency range (stomata were filled with air and hence could not

Table 1
Parameters used in the model.

Parameter	Value
Extracellular liquid conductivity (σ_{ex})	0.0084 S/m (Stout, Hall, & McLaughlin, 1987)
Extracellular liquid permittivity (ε_{ex})	80 (Gavish & Promislow, 2012)
Cell membrane conductivity (σ_m)	0.00003 S/m (Wanichapichart, Bunthawin, Kaewpaiboon, & Kanchanapoom, 2002)
Cell membrane permittivity (ε_m)	10 (Wanichapichart, Bunthawin, Kaewpaiboon & Kanchanapoom, 2002)
Cytoplasm conductivity (σ_{cyt})	0.2 S/m (Harris & Kell, 1983)
Cytoplasm permittivity (ε_{cyt})	80 (Asami, Hanai, & Koizumi, 1980)
Cuticular wax layer conductivity (σ_{cut})	5×10^{-8} S/m (Ramos-Barrado, Benavente & Heredia, 1993), 5×10^{-7} S/m
Cuticular wax layer permittivity (ε_{cut})	10, 45, 80 (Gavish & Promislow, 2012)
Air conductivity (σ_{air})	8×10^{-15} S/m (Pawar, Murugavel, & Lal, 2009)
Air permittivity (ε_{air})	1.006 (Hector & Schultz, 1936)
Impregnating solution conductivity (σ_{im})	0.25 S/m
Impregnating solution permittivity (ε_{im})	80 (Gavish & Promislow, 2012)
Electroporation parameter (α)	10^9 m^{-2} s^{-1} (DeBruin & Krassowska, 1999)
Characteristic voltage of electroporation (V_{ep})	0.258 V (DeBruin & Krassowska, 1999)
Electroporation constant (q)	2.46 (DeBruin & Krassowska, 1999)
Equilibrium pore density (N_0)	1.5×10^9 m^{-2} (DeBruin & Krassowska, 1999)
Energy barrier within pore (w)	2.65 (DeBruin & Krassowska, 1999)
Pore radius (r_p)	0.76 nm (DeBruin & Krassowska, 1999)
Relative entrance length of pores (n)	0.15 (DeBruin & Krassowska, 1999)

contribute to the calculated increase in conductivity). This also explains why models A–C, although possessing different cell sizes and arrangements, responded similarly; the polarization of cell membranes (known as the Maxwell–Wagner effect) does not considerably affect the calculated overall conductivity of the leaf at this frequency range.

One can also note that at high frequencies (>10 kHz) model D with cuticular wax layer gives similar results as models A, B and C without cuticular wax. This means that at these frequencies, the cuticular wax becomes electrically 'transparent' and the rest of the leaf tissues determine the leaf conductivity. Since the values predicted by the model are lower compared to the measured conductivity for frequencies above 10 kHz, apparently the model underestimates the overall conductivity of internal leaf tissues. This may be due to different factors such as the number of cell membranes, cell volumes, as well as extra- and intracellular conductivities. An important factor influencing the disagreement between the data obtained theoretically and experimentally may also be the connections between the cells. In the plant tissue all cells are connected by the plasmodesmata for the proper functioning of the whole organism. The symplast, which is the continuum created by the connected cytoplasms, is not included in the model, since the cells are modeled as membrane-separated elements. The symplast may influence the electrical properties of the tissue by creating additional conductive pathways to the apoplast.

The air fraction is clearly another factor influencing the disparity of the theoretical and experimental results. The average amount of air in the tissue is known, however the location and the size of the air spaces are not uniform in the highly unorganized structure, while in the model the structure is simplified and symmetrical.

Moreover, there are assumptions made considering the conductivities of the cytoplasm and extracellular liquid. The values are taken from previously published data (Table 1), which may also introduce certain differences between the theoretical and experimental data.

5.2. Influence of the air fraction on the conductivity of the spinach leaf

To avoid the randomness introduced by the air fraction in plant tissues, a model without the air fraction was created and investigated. The model of vacuum impregnated leaf is simpler, and hence, less random than the model of non-treated leaf as the connections between cells and the air fraction is removed. The air fraction was exchanged

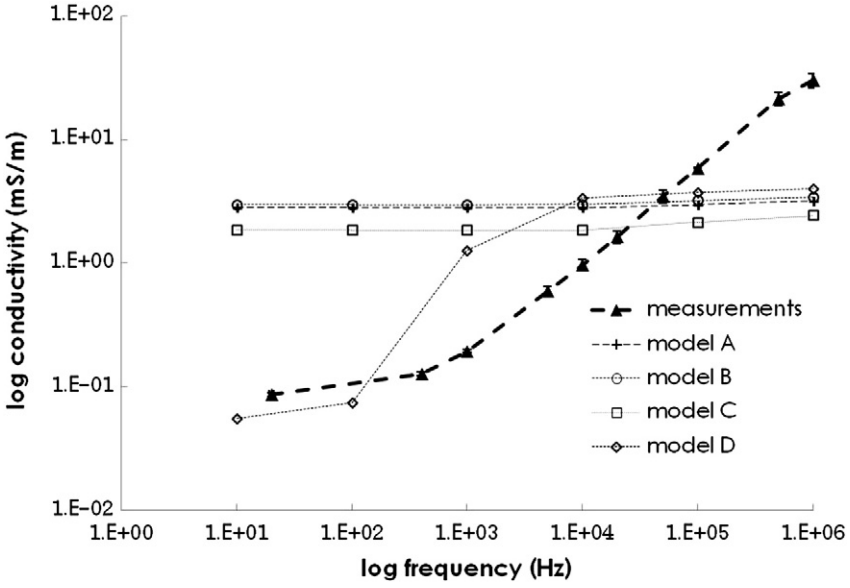

Fig. 3. Comparison of the conductivity changes over the frequency range for experimental measurements and 4 different models with different arrangements of cells in the spongy mesophyll represented in Fig. 2. Error bar represents standard deviation of three replicates.

with a solution of 0.25 S/m conductivity. The model was compared to the experimental data obtained by investigating the conductivity of the leaf samples after vacuum impregnation. For investigating the vacuum impregnated leaf, model D was chosen (4 rows, 4 cells per row). Opened stomata after vacuum impregnation (which were observed under the microscope — results not shown) suggest that they were not fully flooded with buffer after the vacuum impregnation process (Sibbernsen & Mott, 2010). Therefore, in the model representing the vacuum impregnated leaf (without air fraction) stomata were filled with air.

In Section 5.1. we stressed the important influence of the cuticular wax layer on the overall conductivity of the leaf. However, to the best of our knowledge, there are no studies describing the conductivity and permittivity of the spinach cuticular wax layer. For this reason we tested different values of cuticular wax conductivity and permittivity and compared the calculated results with experimental measurements. The conductivity of tomato cuticular wax, 5×10^{-8} S/m, was taken as a reference from the existing literature (Ramos-Barrado, Benavente, & Heredia, 1993), and in addition, a higher conductivity of 5×10^{-7} S/m was also tested. The relative permittivity of the cuticular wax was investigated in the range from 10 to 80, since it is composed from a cuticle matrix with a relative permittivity of approximately 10, containing aqueous pores filled with ionic solutes with relative permittivity of approximately 80 (Schönherr, 2006).

Fig. 4 shows the comparison of the theoretical and experimental data of the vacuum impregnated leaf. The measured conductivity increases with frequency (bold dashed line, Fig. 4). All of the tested values of cuticular wax conductivity and relative permittivity reasonably agreed with the measurements. However, the model using 5×10^{-7} S/m (dashed line B, Fig. 4) had the best prediction of the conductivity values at low frequencies (10–1000 Hz). The final conductivity (at 1 MHz) is similar (90.2–99.8 mS/m) for all tested conductivities and permittivities of the wax layer, consistent with the previously noted observation that the cuticular wax becomes electrically 'transparent' at this frequency, and its influence on the overall leaf conductivity is negligible. The wider transition of the frequency-dependent increase in the measured data compared to model predictions is also indicative of multiple relaxation processes, which could be described by a constant phase element, such as for tomato cuticle (Ramos-Barrado, Benavente & Heredia, 1993).

Indeed, the model of vacuum impregnated leaf even slightly overestimates the measured conductivity at 1 MHz. In the model an ideal process of vacuum impregnation (100% of the air is replaced by the solution) is considered, which may have contributed to the observed discrepancy between the models and experimental data. It was observed that when spinach leaves were impregnated with a sugar solution and examined with micro-X-ray tomography (Panarese, unpublished data), random air pockets remained in the structure accounting for approximately 2–3% of the total volume. These air pockets would decrease the general conductivity of the leaf.

5.3. Electroporation of the spinach leaf cross section

Electroporation of the vacuum impregnated spinach tissue was investigated and compared with the theoretical results by measuring the electric current during the pulse at applied voltages from 50 to 500 V (Fig. 6). Since the leaf is covered with a cuticular wax layer of high resistance, the stomata seem to play a critical role in the electric field distribution within the leaf and the current flow through the leaf cross section.

Stomata were investigated in two hypothetical situations (i) with air in the stomata. This scenario is supported by microscopic observations (Fig. 5A), done as described by Dymek, Dejmek and Gómez Galindo (2014), showing opened stomata (marked with arrows) after vacuum impregnation. According to Sibbernsen and Mott (2010) stomata would close if totally flooded with solution. (ii) It is assumed that electroporation provokes leakage from electroporated cells with a consequent temporal wetting of the solution of the guard cells of stomata. This scenario is supported by microscopic observations (Fig. 5B) showing electroporated guard cells when propidium iodide was used as an electroporation indicator (Dymek, Dejmek & Gómez Galindo, 2014). With pulse amplitudes of 200 V–500 V all the guard cells were uniformly electroporated within the leaf samples (Fig. 5B). With pulse amplitude of 100 V, some of the guard cells in the leaf sample were not electroporated and with pulse amplitude of 50 V, none of the observed guard cells were electroporated. Electric current values obtained by the models at 50 and 100 V are enclosed within the error bars of the measurements. Cells wetting by electroporation may be regarded as temporal as it is well known that a cell membrane that is partially damaged has the ability to recover even if the damage has caused enhanced ion leakage. ATPase activity will help the cell to take up leaked ions against the concentration gradient (Arora & Palta, 1991). We have here considered the application of a single pulse. It is worth to underline that if a train of pulses would be applied to cause reversible permeabilization, the first pulse or pulses affecting stomata will change the modeling situation from a tissue with air-filled stomata to a tissue with stomata filled with cell sap.

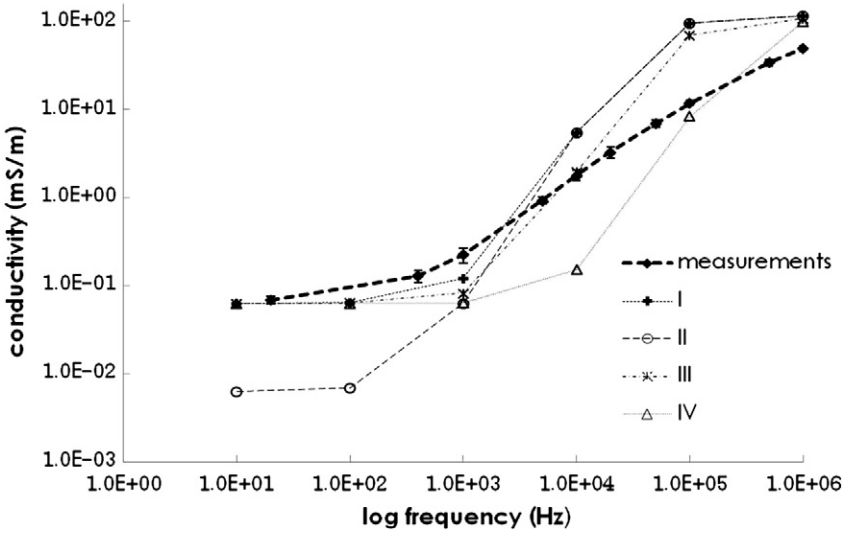

Fig. 4. The measured conductivity of vacuum impregnated spinach leaves compared with the model solved for different values of the conductivity (σ) and permittivity (ε) of the cuticular wax layer: I. $\varepsilon = 80, \sigma = 5 \times 10^{-7}$ S/m II. $\varepsilon = 80, \sigma = 5 \times 10^{-8}$ S/m III. $\varepsilon = 45, \sigma = 5 \times 10^{-7}$ S/m IV. $\varepsilon = 10, \sigma = 5 \times 10^{-7}$ S/m. Error bar represents standard deviation of three replicates.

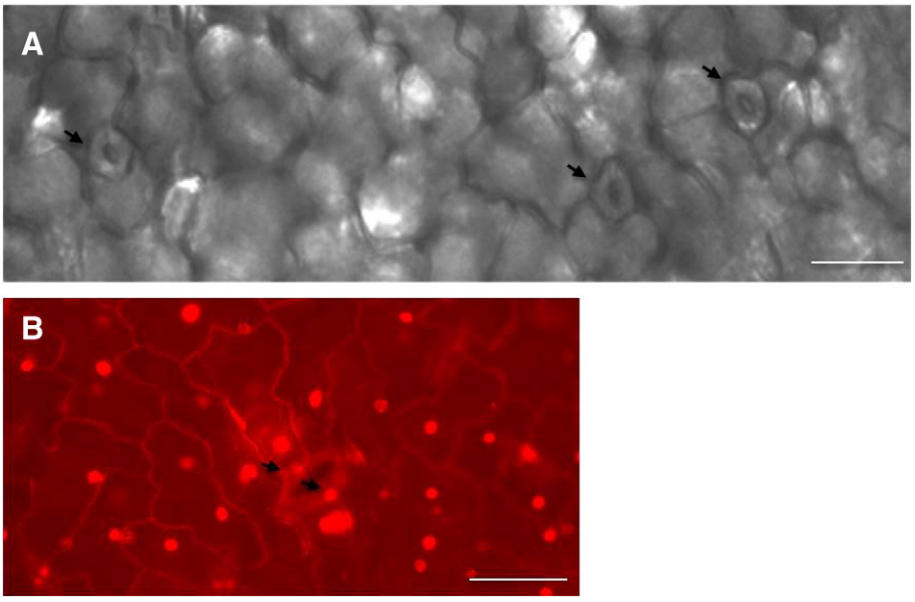

Fig. 5. Representative microscopic pictures showing: A. open stomata after vacuum impregnation process (marked with arrows). B. electroporated guard cells of stomata previously stained with propidium iodide as described in Dymek et al. (2014). One 250 μm rectangular, monopolar pulse with amplitude of 200 V was applied to previously vacuum impregnated leaf. The scale bars represent 20 μm.

In Fig. 6, the current predicted for the two models based on the hypothetical situations described above was compared with measured values of the current during the application of the electric pulse. The model with cell sap in stomata shows good agreement between theoretical and experimental values during the application of electric pulses, whereas the model with air in stomata shows significantly lower values than the measurements. The experimentally measured current increased from 0.1 A at 50 V to 4.5 A at 500 V. The model with air in stomata resulted in currents from 0.00055 A at 50 V to 0.0054 at 500 V. The current obtained by solving the model with solution in stomata was 0.33 A at 50 V and it increased up to 3.9 A at 500 V.

Fig. 7 shows the calculated values of the resistance (i.e. inversed value of conductance) of the spinach leaf cross section for voltages from 50 to 500 V. The resistance was calculated from measured current by $R = V/I$, where R — resistance (Ω), V — voltage (V), and I — current (A). The resistance decreased significantly as the voltages applied were increased from 50 to 300 V and did not further decrease with increasing amplitude of pulses from 300 V to 500 V. Electroporation of the cell membranes causing the decrease of resistance is accompanied by the increasing number of the average pore density calculated by the model (Fig. 7). Fig. 7 also shows that pore density increases markedly in the range from 50 V to 300 V for both models. At applied voltages in the range from 300 V to 500 V pore density however is not further increased. We can conclude that the evolution of pore density corresponds well to the observed decrease in resistance as the function of the applied pulse amplitude.

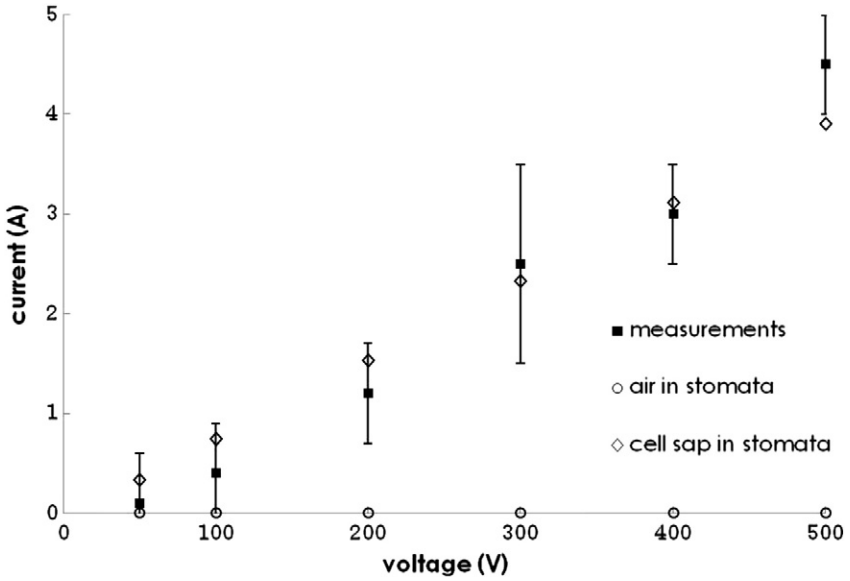

Fig. 6. The measured electric current through vacuum impregnated spinach leaf at different applied voltages, compared with the model solved for two different situations in which stomata are either filled with air or with leaked cell sap from electroporated guard cells. Error bar represents standard deviation of three replicates.

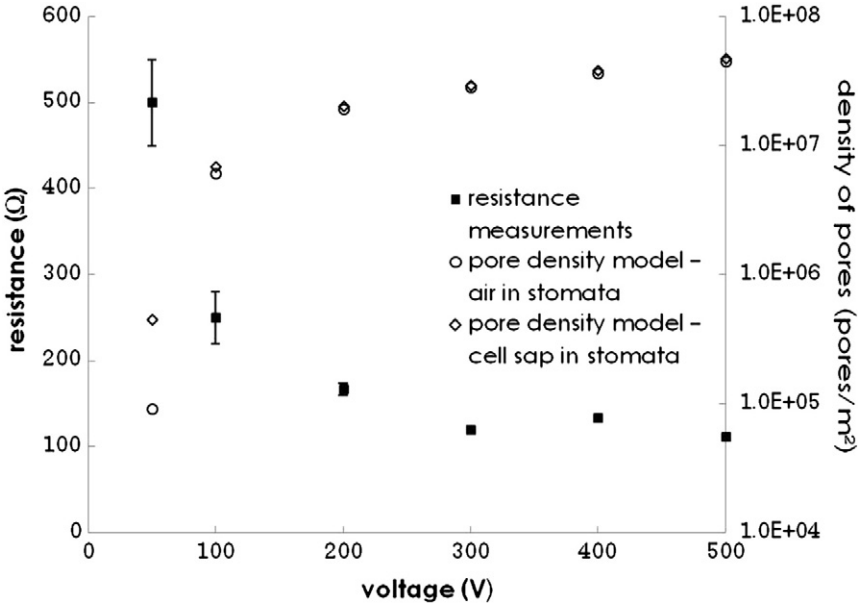

Fig. 7. Calculated average pore density from two models and change in resistance with increasing voltage. The resistance at different applied voltages is plotted together with calculated average pore density for the entire leaf section for two models: air in stomata and call sap in stomata. Resistance was calculated from measured current by R = V/I, where R — resistance (Ω), V — voltage (V), and I — current (A).

A detailed representation of pore density at various applied voltages, indicating electroporation of the different types of cells in the entire cross section of the leaf, was calculated as described by DeBruin and Krassowska (1999) and is shown in Fig. 8. The density of pores is compared between the model with air and the model with cell sap in the stomata. The main difference in pore density can be seen at 50 V, where the model with cell sap in the stomata results in higher pore density than the model with stomata filled with air.

Even if the two tested models show very different results on the changes of current with increasing voltage (Fig. 6), the pore density in the range from 100 to 500 V is similar for the model with air in stomata and for the model with cell sap in stomata (Fig. 8). Since the resistance of the outer layers (upper and lower cuticular wax) is significantly higher than the interior of the leaf cross section (epidermal, mesophyll cells and solution surrounding the cells) the current is determined by the stomata filled either with air or cell sap. However, the pore density is not influenced by the change of settings in the models (air in stomata or cell sap in stomata) due to the still significantly higher resistance of the cuticular wax layer from the internal tissues, regardless of how stomata is filled.

At 50 V the model with air filled stomata is electroporated only at the external surface of the epidermal cells, while the spongy and palisade mesophyll is slightly electroporated. The model with solution in the stomata shows that at 50 V the epidermal cells are electroporated mostly at the surface but also the internal tissues (palisade and spongy mesophyll) are electroporated showing higher pore density than that for the model with air in the stomata. Worth highlighting is the different pattern of pore formation at 50 V. For the model with stomata filled with air electroporation starts at the central part of the epidermal cells surface, while in the model with stomata filled with solution the pores are created around the stomata and at the central part of the epidermal cells surface. With higher voltages (100–500 V) the density of pore increases uniformly in all tissue types. Interesting, the progression of pores density with higher applied voltage (from 100 V to 500 V) is similar for both models. At 100 V the cells of all the tissue types are electroporated at the poles facing the electric field direction. At 200 V it can be seen that the spongy mesophyll cells are uniformly electroporated, while for the palisade mesophyll cells higher pore density is still visible at the poles than at the sides. With higher voltages (300–500 V) the pore density becomes uniform for all the cells.

6. Conclusions

This study has focused on modeling electroporation of the complex heterogeneous structure of spinach leaves. The following remarks underline important findings:

1. In the model of vacuum impregnated leaf, the impregnating solution considerably contributes to the conductive pathways through the leaf cross section. The frequency-dependent conductivity obtained with the model of vacuum impregnated leaf agrees well with the measurements. In the model of nontreated leaf, however, the extent of conductive pathways was probably underestimated.
2. The general conductivity of the leaf is significantly determined by the low conductive wax layer. Since stomata are 'holes' in the wax layer, they play a crucial role in the current flow throughout the leaf cross section. The current is, therefore, markedly affected if stomata are filled with air/gas or cell sap.
3. This theoretical investigation of electroporation shows that, under the investigated PEF conditions, pores start to be created in the membranes of epidermal cells at low voltages (50 V) and with higher voltages the pore density becomes uniform in the entire leaf cross section.

Acknowledgments

This work was in part supported by the Slovenian Research Agency (ARRS) with program numbers P2-0249 and IP-0510. Research was conducted within the scope of the European Associated Laboratory for Pulsed Electric Field Applications in Biology and Medicine (LEA EBAM).

The article is a result of the networking efforts of COST Action TD1104 (www.electroporation.net). Part of the calculations and experimental work was performed during the Short-Term Scientific Mission (Grant ECOST-STSM-TD1104-030912-021795, to Katarzyna Dymek).

The research which led us to these results received funding from the European Community's Seventh Framework Program (FP7/2007-2013) under grant agreement no. 245280, also known under the acronym PRESERF.

Authors would also like to express their deep appreciation to Dr. Matej Reberšek and Dr. Nataša Pavšelj for their initial help with measurements and modeling, respectively.

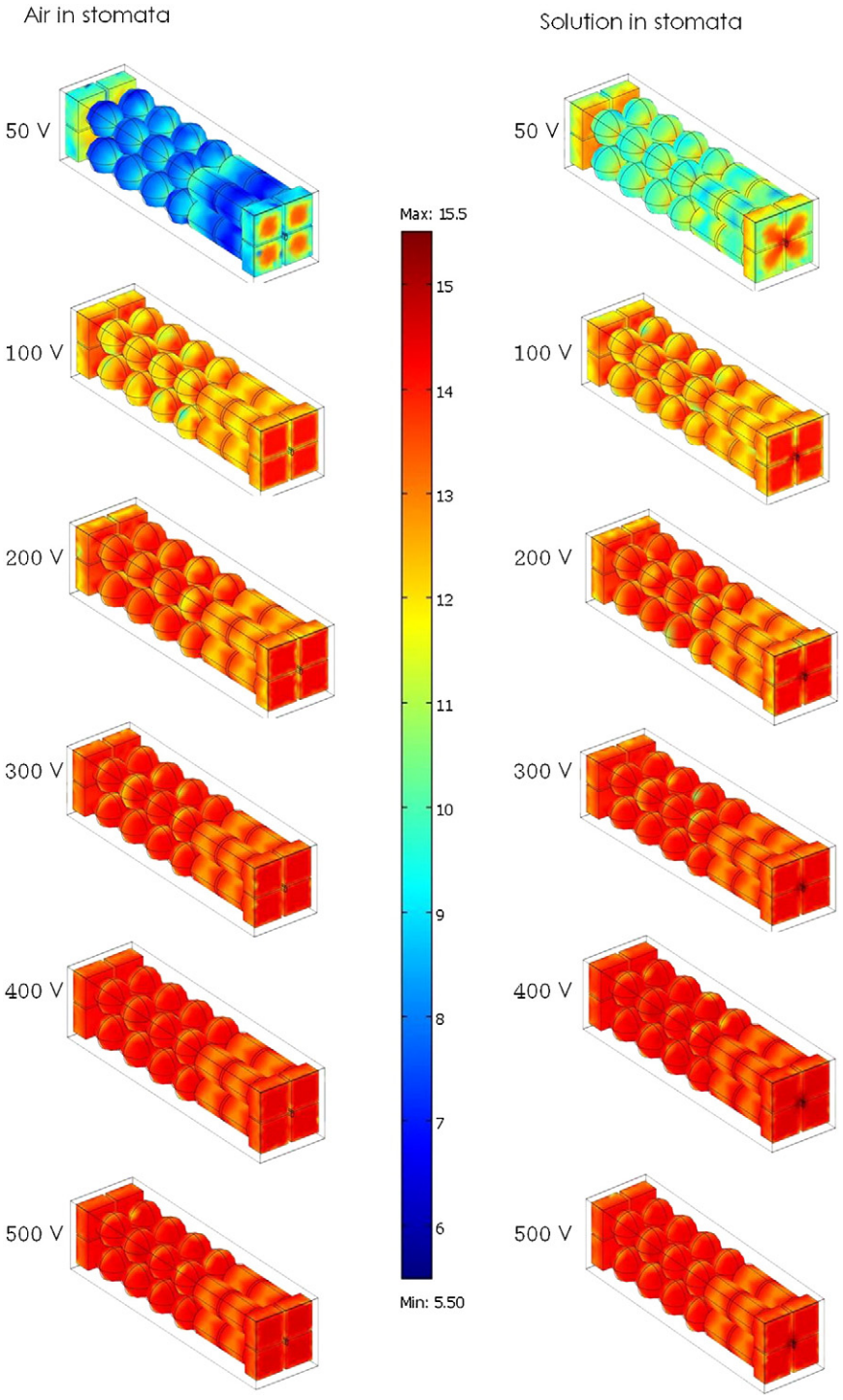

Fig. 8. Distribution of pore density in the electroporated cells investigated with the model of vacuum impregnated spinach leaf after applying electric pulses with different amplitudes. Models, where the stomata are either filled with solution or with air, were investigated. The color scale is logarithmic, from dark blue representing low pore density, to dark red representing high pore density. Pore density is shown in pores/m^2.

References

Arena, C. B., Sano, M. B., Rylander, M. N., & Davalos, R. V. (2011). Theoretical considerations of tissue electroporation with high-frequency bipolar pulses. *IEEE Transactions on Biomedical Engineering, 58*, 1474–1482.

Arora, R., & Palta, J. P. (1991). A loss in the plasma membrane ATPase activity and its recovery coincides with incipient freeze–thaw injury and postthaw recovery in onion bulb scale tissue. *Plant Physiology, 95*, 846–852.

Asami, K., Hanai, T., & Koizumi, N. (1980). Dielectric approach to suspensions of ellipsoidal particles covered with a shell in particular reference to biological cells. *Japanese Journal of Applied Physics, 19*, 359–365.

Corovic, S., Zupanic, A., Kranjc, S., Al Sakere, B., Leroy-Willig, A., Mir, L. M., et al. (2010). The influence of skeletal muscle anisotropy on electroporation: In vivo study and numerical modeling. *Medical & Biological Engineering & Computing, 48*, 637–648.

Daniels, C., & Rubinsky, B. (2009). Electrical field and temperature model of nonthermal irreversible electroporation in heterogeneous tissues. *Journal of Biomechanical Engineering, 131*.

DeBruin, K. A., & Krassowska, W. (1999). Modeling electroporation in a single cell. I. Effects of field strength and rest potential. *Biophysical Journal, 77*, 1213–1224.

Demir, E. (2012). *Optimization of vacuum impregnation and pulsed electric field parameters for improving the cryoprotection of spinach leaves.* (Master Thesis). Lund University.

Dymek, K., Dejmek, P., & Gómez Galindo, F. (2014). Influence of pulsed electric field protocols on the reversible permeabilization of rucola leaves. *Food and Bioprocess Technology*, *7*, 761–773.

Gavish, N., & Promislow, K. (2012). Dependence of the dielectric constant of electrolyte solutions on ionic concentration. arXiv:1208.5169 ([physics.chem-ph]. Retrieved from http://arxiv.org/abs/1208.5169).

Glaser, R., Leikin, S., Chernomordik, L., Pastushenko, V., & Sokirko, A. (1988). Reversible electrical breakdown of lipid bilayers — Formation and evolution of pores. *Biochimica et Biophysica Acta*, *940*, 275–287.

Gowrishankar, T. R., Esser, A. T., Vasilkoski, Z., Smith, K. C., & Weaver, J. C. (2006). Microdosimetry for conventional and supra-electroporation in cells with organelles. *Biochemical and Biophysical Research Communications*, *341*, 1266–1276.

Hardin, J. A., Jones, C. L., Weckler, P. R., Maness, N. O., Dillwith, J. W., & Madden, R. D. (2013). Rapid quantification of spinach leaf cuticular wax using Fourier transform infrared attenuated total reflectance spectroscopy. *Transactions of the ASABE*, *56*, 331–339.

Harris, C. M., & Kell, D. B. (1983). The radio-frequency dielectric properties of yeast cells measured with a rapid, automated, frequency-domain dielectric spectrometer. *Bioelectrochemistry and Bioenergetics*, *11*, 15–28.

Hector, L. G., & Schultz, H. L. (1936). The dielectric constant of air at radiofrequencies. *Physics*, *7*, 133–136.

Kandušer, M., & Miklavčič, D. (2008). Electroporation in biological cell and tissue: An overview. In E. Vorobiev, & N. Lebovka (Eds.), *Electrotechnologies for extraction from food plants and biomaterials food engineering series* (pp. 1–37). New York: Springer.

Kotnik, T., Kramar, P., Pucihar, G., Miklavcic, D., & Tarek, M. (2012). Cell membrane electroporation — Part 1: The phenomenon. *IEEE Electrical Insulation Magazine*, *28*, 14–23.

Mezeme, M. E., Pucihar, G., Pavlin, M., Brosseau, C., & Miklavčič, D. (2012). A numerical analysis of multicellular environment for modeling tissue electroporation. *Applied Physics Letters*, *100*, 143701.

Miklavčič, D., Serša, G., Brecelj, E., Gehl, J., Soden, D., Bianchi, G., et al. (2012). Electrochemotherapy: Technological advancements for efficient electroporation-based treatment of internal tumors. *Medical & Biological Engineering & Computing*, *50*, 1213–1225.

Neumann, E., & Rosenheck (1972). Permeability changes induced by electric impulses in vesicular membranes. *Journal of Membrane Biology*, *10*, 279–290.

Neumann, E., Schaefer-Ridder, M., Wang, Y., & Hofschneider, P. (1982). Gene transfer into mouse lyoma cells by electroporation in high electric fields. *EMBO Journal*, *1*, 841–845.

Panarese, V., Dejmek, P., Rocculi, P., & Gómez Galindo, F. (2013). Microscopic studies providing insight into the mechanisms of mass transfer in vacuum impregnation. *Innovative Food Science & Emerging Technologies*, *18*, 169–176.

Pavliha, D., Kos, B., Zupanič, A., Marčan, M., Serša, G., & Miklavčič, D. (2012). Patient-specific treatment planning of electrochemotherapy: Procedure design and possible pitfalls. *Bioelectrochemistry*, *87*, 265–273.

Pavšelj, N., & Miklavčič, D. (2008). Numerical modeling in electroporation-based biomedical applications. *Radiology and Oncology*, *42*, 159–168.

Pavšelj, N., & Miklavčič, D. (2011). Resistive heating and electropermeabilization of skin tissue during in vivo electroporation: A coupled nonlinear finite element model. *International Journal of Heat and Mass Transfer*, *54*, 2294–2302.

Pawar, S. D., Murugavel, P., & Lal, D.M. (2009). Effect of relative humidity and sea level pressure on electrical conductivity of air over Indian Ocean. *Journal of Geophysical Research*, *114* (D02205).

Phillips, M., Maor, E., & Rubinsky, B. (2011). Principles of tissue engineering with nonthermal irreversible electroporation. *Journal of Heat Transfer—Transactions of the ASME*, *133*, 011004.

Phoon, P. Y., Gómez Galindo, F., Vicente, A., & Dejmek, P. (2008). Pulsed electric field in combination with vacuum impregnation with trehalose improves the freezing tolerance of spinach leaves. *Journal of Food Engineering*, *88*, 144–148.

Pucihar, G., Miklavcic, D., & Kotnik, T. (2009). A time-dependent numerical model of transmembrane voltage inducement and electroporation of irregularly shaped cells. *IEEE Transactions on Biomedical Engineering*, *56*, 1491–1501.

Ramos-Barrado, J., Benavente, J., & Heredia, A. (1993). Electrical conductivity of differently treated isolated cuticular membranes by impedance spectroscopy. *Archives of Biochemistry and Biophysics*, *306*, 337–341.

Retelj, L., Pucihar, G., & Miklavcic, D. (2013). Electroporation of intracellular liposomes using nanosecond electric pulses — A theoretical study. *IEEE Transactions on Biomedical Engineering*, *60*, 2624–2635.

Riederer, M., & Schreiber, L. (2001). Protecting against water loss: Analysis of the barrier properties of plant cuticles. *Journal of Experimental Botany*, *52*, 2023–2032.

Rowan, N. J., MacGregor, S. J., Anderson, J. G., Fouracre, R. A., & Farish, O. (2000). Pulsed electric field inactivation of diarrhoeagenic *Bacillus cereus* through irreversible electroporation. *Letters in Applied Microbiology*, *31*, 110–114.

Saulis, G. (1997). Pore disappearance in a cell after electroporation: Theoretical simulation and comparison with experiments. *Biophysical Journal*, *73*, 1299–1309.

Schönherr, J. (2006). Characterization of aqueous pores in plant cuticles and permeation of ionic solutes. *Journal of Experimental Botany*, *57*, 2471–2491.

Shayanfar, S., Chauhan, O., Toepfl, S., & Heinz, V. (2013). The interaction of pulsed electric fields and texturizing–antifreezing agents in quality retention of defrosted potato strips. *International Journal of Food Science & Technology*, *48*, 1289–1295.

Sibbernsen, E., & Mott, K. A. (2010). Stomatal responses to flooding of the intercellular air spaces suggest a vapor-phase signal between the mesophyll and the guard cells. *Plant Physiology*, *153*, 1435–1442.

Stout, D.G., Hall, J. W., & McLaughlin, N.B. (1987). In vivo plant impedance measurements and characterization of membrane electrical properties: The influence of cold acclimation. *Cryobiology*, *24*, 148–162.

Suzuki, D. O. H., Ramos, A., Ribeiro, M. C. M., Cazarolli, L. H., Silva, F. R. M. B., Leite, L. D., et al. (2011). Theoretical and experimental analysis of electroporated membrane conductance in cell suspension. *IEEE Transactions on Biomedical Engineering*, *58*, 3310–3318.

Talele, S., & Gaynor, P. (2010). Modelling control of pore number and radii distribution in single-cell electroporation. In K. Elleithy, T. Sobh, M. Iskander, V. Kapila, M.A. Karim, & A. Mahmood (Eds.), *Technological developments in networking, education and automation* (pp. 231–236). Netherlands: Springer.

Talele, S., Gaynor, P., Cree, M. J., & van Ekeran, J. (2010). Modelling single cell electroporation with bipolar pulse parameters and dynamic pore radii. *Journal of Electrostatics*, *68*, 261–274.

Wanichapichart, P., Bunthawin, S., Kaewpaiboon, A., & Kanchanapoom, K. (2002). Determination of cell dielectric properties using dielectrophoretic technique. *Science Asia*, *28*, 113–119.

Warmbrodt, R. D., & Woude, W. J. V. (1990). Leaf of *Spinacia oleracea* (Spinach): Ultrastructure, and plasmodesmatal distribution and frequency, in relation to sieve-tube loading. *American Journal of Botany*, *77*, 1361–1377.

Winter, H., Robinson, D.G., & Heldt, H. W. (1994). Subcellular volumes and metabolite concentrations in spinach leaves. *Planta*, *193*, 530–535.

Yarmush, M. L., Golberg, A., Serša, G., Kotnik, T., & Miklavčič, D. (2014). Electroporation-based technologies for medicine: Principles, applications, and challenges. *Annual Review of Biomedical Engineering*, *16*, 295–320.

Zimmermann, U., Pilwat, G., & Riemann, F. (1974). Dielectric breakdown of cell membranes. *Biophysical Journal*, *14*, 881–899.

Zimmermann, U., & Vienken, J. (1982). Electric field-induced cell-to-cell fusion. *Journal of Membrane Biology*, *67*, 165–182.

Zorec, B., Becker, S., Reberšek, M., Miklavčič, D., & Pavšelj, N. (2013). Skin electroporation for transdermal drug delivery: The influence of the order of different square wave electric pulses. *International Journal of Pharmaceutics*, *457*, 214–223.